THE JOURNAL OF PHYSICAL CHEMISTRY B

Article

pubs.acs.org/JPCB

Extension of a Classic Low Frequency Dielectric Dispersion Theory of Colloidal Suspensions to Include Different Counterion and Co-Ion Valences, a Broad Frequency Range, and the Stagnant Layer Conductivity

Constantino Grosse*

Departamento de Física, Universidad Nacional de Tucumán, Av. Independencia 1800, (4000) San Miguel de Tucumán, Argentina, and Consejo Nacional de Investigaciones Científicas y Técnicas, Av. Rivadavia 1917, (C1033AAJ) Buenos Aires, Argentina

ABSTRACT: A unified extension of the classic Shilov–Dukhin theory of the low frequency dielectric dispersion of colloidal dispersions is presented. Purely analytical expressions for the AC dielectric and electrokinetic response over a broad frequency range including different counterion and co-ion valences and the presence of the stagnant layer conductivity are deduced. The obtained results are generally in good to very good agreement with available numerical data, showing that they should be useful for the interpretation of a broad range of experimental results without having to rely on numerical calculations.

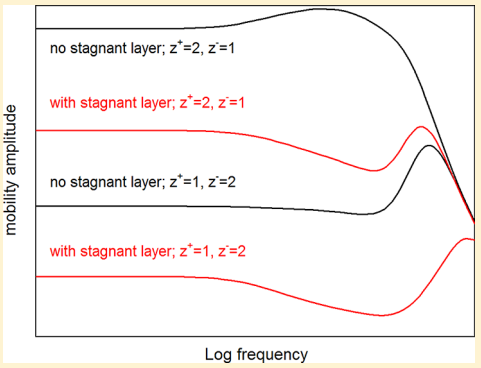

INTRODUCTION

The classical thin double layer concentration polarization theory in colloidal suspensions was first developed by Dukhin and Shilov[1] in the late 1960s. This DC study was extended in the following year to the AC regime, leading to the description of the low frequency dielectric dispersion phenomenon.[2,3] These works were based on the standard electrokinetic model[4] and assumed, furthermore, that the counterion and co-ion valences have the same value: $z^+ = z^-$ (actually, the possible existence of a stagnant layer conductivity was considered in refs 2 and 3 considering that the zero fluid velocity surface might not coincide with the surface of the particle).

In the following years, the main theoretical advances on this subject were of a numerical nature: solution of the whole electrokinetic equation set for arbitrary double layer thickness with an arbitrary number of ionic species and ion valence values in both DC[5] and AC[6] fields, broad frequency range including inertial effects,[7] and stagnant layer conductivity in both DC[8] and AC[9,10] fields. However, the analytical extensions of the original works were much more limited and only approximate in nature. They mainly dealt with different counterion and co-ion valences,[11] the extension of the model validity to the high frequency range,[12,13] and the inclusion of the anomalous surface conductivity.[13−15]

In a recent series of works, we presented extensions of the original models including different counterion and co-ion valences ($z^+ = 2z^-$ and $z^- = 2z^+$) both in DC [16] and low frequency AC,[17] high frequency AC,[18] and stagnant layer conductivity in DC.[19] In this work, we deduce the one extension that was still missing: stagnant layer conductivity in low and high frequency AC. We also extend the previous stagnant layer conductivity DC treatment to include different counterion and co-ion valences. The final result is a fully analytical thin double layer formulation of the dielectric and electrokinetic response of colloidal suspensions both in the DC and broad frequency AC range, including different counterion and co-ion valences and the stagnant layer conductivity. In order to keep the presentation as short as possible, we only include the new aspects of the theory and refer to previous work for the remaining part. However, we do include all the equations needed for the final results in order to be able to use them without having to refer to previous works.

EQUATION SET

The classic Shilov–Dukhin low frequency dielectric dispersion theory is based on the *standard electrokinetic model*,[4] so that the suspended particle is represented by an insulating sphere of radius a, with a uniform fixed surface charge density σ_0. The surrounding electrolyte solution is characterized by its viscosity η_e, absolute permittivity ε_e, the unsigned valences of its ions $z^{\pm}$, their diffusion coefficients $D^{\pm}$, and their number concentrations far from the particle:

$$C^{\pm}(\infty) = z^{\mp}N$$

In this work, we shall extend the standard model by considering, just as in ref 19, that the particle is surrounded by a surface layer of adsorbed ions that can move tangentially with diffusion

Received: July 30, 2012
Revised: October 5, 2012
Published: November 5, 2012

coefficients $D_s^{\pm}$, while the fluid remains immobile. The equilibrium (lower index 0) surface densities are determined by the following adsorption isotherms:[8]

$$C_{s0}^{\pm} = \frac{N_s^{\pm} C_0^{\pm}(a)/K_s^{\pm}}{1 + C_0^{+}(a)/K_s^{+} + C_0^{-}(a)/K_s^{-}} \tag{1}$$

In this equation, $N_s^{\pm}$ are the maximum values of the surface concentrations of adsorbed ions and $K_s^{\pm}$ are their dissociation constants.

Outside the surface layer, the ion concentrations $C^{\pm}(\vec{r}, t)$, electric potential $\Phi(\vec{r}, t)$, fluid velocity $\vec{V}(\vec{r}, t)$, and pressure $P(\vec{r}, t)$ are determined by the usual set of the Nernst−Planck, continuity, Poisson, Navier−Stokes, and incompressibility equations. The full formulation, based on the *thin double layer approximation*

$$\kappa a \gg 1 \tag{2}$$

where

$$\kappa = \sqrt{\frac{z^{+}z^{-}(z^{+} + z^{-})e^2 N}{\varepsilon_e kT}} \tag{3}$$

is the reciprocal Debye length, is presented in detail in ref 17 and outlined in ref 18.

Briefly, the equation set is first solved in equilibrium, which leads to the equilibrium ion concentrations

$$C_0^{\pm} = z^{\mp} N e^{\mp z^{\pm}\tilde{\Phi}_0} \tag{4}$$

to the Poisson−Boltzmann equation for the equilibrium potential

$$\nabla^2 \tilde{\Phi}_0 = -\frac{z^{+}z^{-}e^2 N}{\varepsilon_e kT}(e^{-z^{+}\tilde{\Phi}_0} - e^{z^{-}\tilde{\Phi}_0})$$

and to an expression relating the zeta potential to the electrolyte concentration and the total surface charge density of the particle

$$\sigma_0 + \sigma_{s0}^{+} + \sigma_{s0}^{-} = \mathrm{sign}(\tilde{\zeta})\sqrt{z^{-}e^{-z^{+}\tilde{\zeta}} + z^{+}e^{z^{-}\tilde{\zeta}} - z^{+} - z^{-}} \times \sqrt{2\varepsilon_e kTN} \tag{5}$$

where

$$\sigma_{s0}^{\pm} = \pm z^{\pm} e C_{s0}^{\pm}$$

In these expressions, the tilde "~" denotes a dimensionless magnitude: $\tilde{\Phi} = \Phi e/(kT)$.

When a macroscopic AC electric field $Ee^{i\omega t}$ is applied to the system, the equations are simplified using the *principle of local equilibrium*: each volume element of the system is in a state of equilibrium, even when different volume elements are not in equilibrium with one another. This condition is expressed in terms of a *virtual system*, that is,

(a) electroneutral in its entire volume

$$c^{*\pm} = z^{\mp} n^{*} \tag{6}$$

(b) in equilibrium everywhere with the real system

$$\tilde{\mu}^{*\pm} = \ln \frac{C^{*\pm}}{z^{\mp}N} \pm z^{\pm}\tilde{\Phi}^{*} = \ln \frac{n^{*}}{N} \pm z^{\pm}\tilde{\varphi}^{*} \tag{7}$$

where $c^{*\pm}$ and φ^{*} are the ion concentrations and the electric potential in the virtual system, $\mu^{*\pm}$ are the electrochemical potentials, the asterisk denotes a complex magnitude, and $\tilde{\mu}^{*\pm} = \mu^{*\pm}/(kT)$. Using eqs 6 and 7, the ion concentrations can be expressed in terms of the virtual system parameters:

$$C^{*\pm} = z^{\mp} n^{*} e^{\mp z^{\pm}(\tilde{\Phi}^{*} - \tilde{\varphi}^{*})} \tag{8}$$

The resulting equation set is then linearized, writing each field-dependent magnitude as an expansion in successive powers of the applied field strength, for example:

$$C^{*\pm} = C_0^{\pm} + \delta C^{*\pm} + \ldots$$

where a magnitude preceded by the δ character is linear in the applied field. Combining these expansions with the original equations, dropping all the higher than first order in the applied field terms, and using the equilibrium expressions leads to the final equation set. It is solved outside the equilibrium double layer using the *hypothesis of approximate electroneutrality*: the electrolyte solution that is electroneutral in equilibrium remains electroneutral when an AC field is applied. The obtained solution, valid outside the equilibrium double layer, is

$$\delta\tilde{n}^{*} = K_c^{*} e^{\sqrt{\xi^{*}}\kappa(a-r)}\left(\frac{a}{r}\right)^2 \frac{1 + \sqrt{\xi^{*}}\kappa r}{1 + \sqrt{\xi^{*}}\kappa a}\frac{eEa}{kT}\cos\theta \tag{9}$$

$$\delta\tilde{\Phi}^{*} = \delta\tilde{\varphi}^{*} = \left(\frac{K_d^{*}a^2}{r^2} - \frac{r}{a}\right)\frac{eEa}{kT}\cos\theta + \delta\tilde{n}^{*}\Delta \tag{10}$$

where

$$\delta\tilde{n}^{*} = \delta n^{*}/N$$

$$\xi^{*} = \frac{i\omega}{\kappa^2 D_{ef}}$$

$$\Delta = \frac{D^{-} - D^{+}}{z^{+}D^{+} + z^{-}D^{-}}$$

$$D_{ef} = \frac{(z^{+} + z^{-})D^{+}D^{-}}{z^{+}D^{+} + z^{-}D^{-}}$$

while K_c^{*} and K_d^{*} are the concentration and dipolar integration coefficients.

BOUNDARY CONDITIONS

The coefficients K_c^{*} and K_d^{*} are determined integrating the continuity equations written for the differences between the actual ion flows $\delta\vec{j}^{*\pm}$ and the long-range (lower index l) flows $\delta\vec{j}_l^{*\pm}$ that are calculated using expressions *that are only valid outside the diffuse double layer*:

$$\int_a^{\infty}\left\{\frac{1}{r^2}\frac{\partial}{\partial r}[r^2(\delta j_r^{*\pm} - \delta j_{lr}^{*\pm})] + \frac{1}{r\sin\theta}\frac{\partial}{\partial\theta}[\sin\theta(\delta j_\theta^{*\pm} - \delta j_{l\theta}^{*\pm})]\right\}\mathrm{d}r = -\int_a^{\infty}\frac{\partial}{\partial t}(\delta C^{*\pm} - z^{\mp}N\delta\tilde{n}^{*})\,\mathrm{d}r \tag{11}$$

where

$$\delta\vec{j}^{*\pm} = -C_0^{\pm}D^{\pm}\nabla\delta\tilde{\mu}^{*\pm} + C_0^{\pm}\delta\vec{V}^{*} \tag{12}$$

$$\delta\vec{j}_l^{*\pm} = -z^{\mp}ND^{\pm}\nabla\delta\tilde{\mu}^{*\pm} + z^{\mp}N\delta\vec{V}^{*} \tag{13}$$

$$\delta\tilde{\mu}^{*\pm} = \delta\tilde{n}^{*} \pm z^{\pm}\delta\tilde{\varphi}^{*} \tag{14}$$

dx.doi.org/10.1021/jp3075404 | J. Phys. Chem. B 2012, 116, 13538−13553

The integrals can be analytically evaluated *assuming that the tangential gradient of the electrochemical potential does not change across the thin double layer*. Proceeding exactly as in ref 19 transforms eq 11 into

$$
\begin{aligned}
&-\delta j_r^{*\pm}(a) - z^{\mp}ND^{\pm}\nabla_r\delta\tilde{\mu}^{*\pm}|_a \\
&= \frac{D^{\pm}}{a\sin\theta}\frac{\partial}{\partial\theta}(\sin\theta\,\nabla_\theta\delta\tilde{\mu}^{*\pm}|_a)\int_a^\infty (C_0^{\pm} - z^{\mp}N)\,\mathrm{d}r \\
&\quad - \frac{1}{a\sin\theta}\frac{\partial}{\partial\theta}[\sin\theta\int_a^\infty (C_0^{\pm} - z^{\mp}N)\delta V_\theta^*\,\mathrm{d}r] \\
&\quad - i\omega\int_a^\infty (\delta C^{*\pm} - z^{\mp}N\delta\tilde{n}^*)\,\mathrm{d}r
\end{aligned}
\tag{15}
$$

The first integral in eq 15 represents the nonspecific adsorption coefficients $G_0^{\pm}$ (excess equilibrium surface densities of counterions or co-ions). Their values, calculated in ref 16, are

(11) For $z^+ = z^- = z$

$$
G_0^{11\pm} = \frac{\kappa\varepsilon_e kT}{(ze)^2}(e^{\mp z\tilde{\zeta}/2} - 1) \tag{16}
$$

(21) For $z^+ = 2z^- = 2z$

$$
G_0^{21\pm} = \frac{\kappa\varepsilon_e kT}{(ze)^2}\frac{z^{\mp}}{6z}(e^{\mp z\tilde{\zeta}/2}\sqrt{3e^{-z\tilde{\zeta}} + 6} - 3) \tag{17}
$$

(12) For $2z^+ = z^- = 2z$

$$
G_0^{12\pm} = \frac{\kappa\varepsilon_e kT}{(ze)^2}\frac{z^{\mp}}{6z}(e^{\mp z\tilde{\zeta}/2}\sqrt{3e^{z\tilde{\zeta}} + 6} - 3) \tag{18}
$$

The second integral represents the convective flow of ions along the particle surface, where the fluid velocity $\delta\vec{V}$ is a superposition of electroosmotic and capillary osmotic contributions:

$$
\begin{aligned}
&\int_a^\infty (C_0^{\pm} - z^{\mp}N)\delta V_\theta^*\,\mathrm{d}r \\
&= -\frac{\varepsilon_e N}{\kappa\eta_e}\left(\frac{kT}{e}\right)^2(\nabla_\theta\delta\tilde{\varphi}^* I_{eo}^{\pm} + \nabla_\theta\delta\tilde{n}^* I_{co}^{\pm})
\end{aligned}
$$

The expressions for the coefficients $I_{eo}^{\pm}$ and $I_{co}^{\pm}$ are also given in ref 16 but written in a slightly different form:

(11) For $z^+ = z^- = z$

$$
I_{eo}^{11\pm} = \pm\frac{2\kappa a G_0^{11\pm}}{zNa} + 2z\tilde{\zeta}
$$

$$
I_{co}^{11\pm} = \frac{1}{z}\left\{\pm I_{eo}^{11\pm} + 4\left[z\tilde{\zeta} - 4\ln\left(\frac{1 + e^{z\tilde{\zeta}/2}}{2}\right)\right]\right\}
$$

(21) For $z^+ = 2z^- = 2z$

$$
\begin{aligned}
I_{eo}^{21\pm} = \frac{z^{\mp}}{z}\Bigg[&\pm\frac{\kappa a G_0^{21\pm}}{zNa} + 3z\tilde{\zeta} \\
&+ \sqrt{3}\ln\left(\frac{1 + e^{z\tilde{\zeta}} + \sqrt{1 + 2e^{z\tilde{\zeta}}}}{(2 + \sqrt{3})e^{z\tilde{\zeta}}}\right)\Bigg]
\end{aligned}
$$

$$
\begin{aligned}
I_{co}^{21\pm} = \frac{z^{\mp}}{2z^2}\Bigg\{&\pm I_{eo}^{21\pm} + 3\Bigg[3z\tilde{\zeta} \\
&+ \sqrt{3}\ln\left(\frac{1 + e^{z\tilde{\zeta}} + \sqrt{1 + 2e^{z\tilde{\zeta}}}}{(2 + \sqrt{3})e^{z\tilde{\zeta}}}\right) \\
&+ 6\ln\left(\frac{6}{2 + e^{z\tilde{\zeta}} + \sqrt{3 + 6e^{z\tilde{\zeta}}}}\right)\Bigg]\Bigg\}
\end{aligned}
$$

(12) For $2z^+ = z^- = 2z$

$$
\begin{aligned}
I_{eo}^{12\pm} = \frac{z^{\mp}}{z}\Bigg[&\pm\frac{\kappa a G_0^{12\pm}}{zNa} + 3z\tilde{\zeta} \\
&- \sqrt{3}\ln\left(\frac{1 + e^{-z\tilde{\zeta}} + \sqrt{1 + 2e^{-z\tilde{\zeta}}}}{(2 + \sqrt{3})e^{-z\tilde{\zeta}}}\right)\Bigg]
\end{aligned}
$$

$$
\begin{aligned}
I_{co}^{12\pm} = \frac{z^{\mp}}{2z^2}\Bigg\{&\pm I_{eo}^{12\pm} - 3\Bigg[3z\tilde{\zeta} \\
&- \sqrt{3}\ln\left(\frac{1 + e^{-z\tilde{\zeta}} + \sqrt{1 + 2e^{-z\tilde{\zeta}}}}{(2 + \sqrt{3})e^{-z\tilde{\zeta}}}\right) \\
&- 6\ln\left(\frac{6}{2 + e^{-z\tilde{\zeta}} + \sqrt{3 + 6e^{-z\tilde{\zeta}}}}\right)\Bigg]\Bigg\}
\end{aligned}
$$

The first addend in eq 15 can be expressed in terms of the stagnant layer parameters using the continuity equation:

$$
\nabla_\theta\cdot\delta j_s^{*\pm} + \delta j_r^{*\pm}(a) = -i\omega\delta C_s^{*\pm} \tag{19}
$$

where

$$
\delta j_s^{*\pm} = \frac{D_s^{\pm}C_{s0}^{\pm}}{a}\left(\frac{\delta\tilde{C}_s^{*\pm} \pm z^{\pm}\delta\tilde{\Phi}^*(a)}{\cos\theta}\right)\sin\theta \tag{20}
$$

are the surface flows of ions in the stagnant layer and

$$
\delta\tilde{C}_s^{*\pm} = \delta C_s^{*\pm}/C_{s0}^{\pm}
$$

are the relative field-induced changes of the adsorbed ion concentrations. Note that eq 20 corrects a mistake in the $\cos\theta$ dependence of the corresponding equation in ref 19. Combining eqs 19 and 20 leads to

$$
\delta j_r^{*\pm}(a) = -\frac{2D_s^{\pm}C_{s0}^{\pm}}{a^2}[\delta\tilde{C}_s^{*\pm}(1 + i\omega\tau_s^{\pm}) \pm z^{\pm}\delta\tilde{\Phi}^*(a)]
$$

where

$$
\tau_s^{\pm} = a^2/(2D_s^{\pm})
$$

are relaxation times associated with the stagnant layer. Using these results together with eq 14 transforms eq 15 into

dx.doi.org/10.1021/jp3075404 | J. Phys. Chem. B 2012, 116, 13538−13553

$$-z^{\mp}ND^{\pm}\nabla_r\delta\tilde{\mu}^{*\pm}|_a = -\frac{2D^{\pm}G_0^{\pm}}{a^2}[\delta\tilde{n}^*(a) \pm z^{\pm}\delta\tilde{\varphi}^*(a)] - \frac{2D_s^{\pm}C_{s0}^{\pm}}{a^2}[\delta\tilde{C}_s^{*\pm}(1 + i\omega\tau_s^{\pm}) \pm z^{\pm}\delta\tilde{\Phi}^*(a)] + \frac{\varepsilon_e N}{\kappa\eta_e}\left(\frac{kT}{e}\right)^2\frac{1}{a\sin\theta} \times \frac{\partial}{\partial\theta}[\sin\theta(I_{eo}^{\pm}\nabla_\theta\delta\tilde{\varphi}^*|_a + I_{co}^{\pm}\nabla_\theta\delta\tilde{n}^*|_a)] - i\omega\int_a^\infty(\delta C^{*\pm} - z^{\mp}N\delta\tilde{n}^*)\,dr \quad (21)$$

Except for the presence of the asterisks, the different ion valences, and the terms proportional to $i\omega$, this equation has exactly the same form as in the DC case, eq 33 in ref 19.

In order to proceed, it is necessary to determine the expression for the field-induced changes of the stagnant layer ion concentrations $\delta C_s^{\pm}$. We shall assume as in ref 10 that, in the considered frequency range, *the characteristic times of the adsorption−desorption processes of cations and anions are much smaller than the period of the applied electric field*. Under this assumption, the equilibrium adsorption isotherms are also valid out of equilibrium, just as in the DC case:[8,19]

$$C_s^{*\pm} = \frac{N_s^{\pm}C^{*\pm}(a)/K_s^{\pm}}{1 + C^{*+}(a)/K_s^{+} + C^{*-}(a)/K_s^{-}} \quad (22)$$

so that

$$\delta\tilde{C}_s^{*\pm} = \delta\tilde{C}^{*\pm}(a) - \tilde{C}_{s0}^{+}\delta\tilde{C}^{*+}(a) - \tilde{C}_{s0}^{-}\delta\tilde{C}^{*-}(a)$$

In this expression,

$$\delta\tilde{C}^{*\pm} = \delta C^{*\pm}/C_0^{\pm}$$

$$\tilde{C}_{s0}^{\pm} = C_{s0}^{\pm}/N_s^{\pm}$$

while the field-induced ion concentration changes at the inner boundary of the diffuse double layer $\delta C^{*\pm}(a)$ are deduced from the local equilibrium condition, eq 8:

$$\delta\tilde{C}^{*\pm}(a) = \delta\tilde{n}^*(a) \mp z^{\pm}[\delta\tilde{\Phi}^*(a) - \delta\tilde{\varphi}^*(a)]$$

The term associated with the stagnant layer in eq 21 so becomes

$$\delta\tilde{C}_s^{*\pm}(1 + i\omega\tau_s^{\pm}) \pm z^{\pm}\delta\tilde{\Phi}^*(a) = (1 + i\omega\tau_s^{\pm})[(1 - \tilde{C}_{s0}^{+} - \tilde{C}_{s0}^{-})\delta\tilde{n}^*(a) \pm (1 \mp \tilde{C}_{s0}^{+} \pm \tilde{C}_{s0}^{-})z^{\pm}\delta\tilde{\varphi}^*(a)] + [(1 + i\omega\tau_s^{\pm})(\tilde{C}_{s0}^{+} - \tilde{C}_{s0}^{-}) \mp i\omega\tau_s^{\pm}]z^{\pm}\delta\tilde{\Phi}^*(a) \quad (23)$$

Next, an expression for the field-induced potential change at the inner boundary of the diffuse double layer $\delta\tilde{\Phi}^*(a)$ is needed. Note that inside the diffuse double layer $\delta\tilde{\Phi}^*$ depends on the distance to the particle, unlike $\delta\tilde{\varphi}^*$ and $\delta\tilde{n}^*$ that are classically considered to remain constant across the thin double layer in view of the local equilibrium condition and eq 2. The potential change $\delta\tilde{\Phi}^*(a)$ can be expressed as the sum of $\delta\tilde{\varphi}^*(a)$ plus a contribution dependent on the concentration change. This contribution can be determined combining eqs 4, 5, and 22, which leads to

$$z^{\pm}\delta\tilde{\Phi}^*(a) = z^{\pm}\delta\tilde{\varphi}^*(a) - S^{\pm}\delta\tilde{n}^*(a) \quad (24)$$

where

$$S^{\pm} = z^{\pm}\frac{\mathrm{sign}(\tilde{\zeta})\sqrt{\varepsilon_e kTN/2}\sqrt{z^-e^{-z^+\tilde{\zeta}} + z^+e^{z^-\tilde{\zeta}} - z^+ - z^-} - (z^+eC_{s0}^{+} - z^-eC_{s0}^{-})(1 - \tilde{C}_{s0}^{+} - \tilde{C}_{s0}^{-})}{\mathrm{sign}(\tilde{\zeta})\sqrt{\varepsilon_e kTN/2}\frac{z^+z^-(e^{z^-\tilde{\zeta}} - e^{-z^+\tilde{\zeta}})}{\sqrt{z^-e^{-z^+\tilde{\zeta}} + z^+e^{z^-\tilde{\zeta}} - z^+ - z^-}} + z^+eC_{s0}^{+}[z^+(1 - \tilde{C}_{s0}^{+}) + z^-\tilde{C}_{s0}^{-}] + z^-eC_{s0}^{-}[z^+\tilde{C}_{s0}^{+} + z^-(1 - \tilde{C}_{s0}^{-})]}$$

This transforms eq 24 into

$$\delta\tilde{C}_s^{*\pm}(1 + i\omega\tau_s^{\pm}) \pm z^{\pm}\delta\tilde{\Phi}^*(a) = M^{*\pm}\delta\tilde{n}^*(a) \pm z^{\pm}\delta\tilde{\varphi}^*(a) \quad (25)$$

where

$$M^{*\pm} = M^{\pm} + i\omega\tau_s^{\pm}(M^{\pm} \pm S^{\pm}) \quad (26)$$

while

$$M^{\pm} = 1 - \tilde{C}_{s0}^{+}(1 + S^{\pm}) - \tilde{C}_{s0}^{-}(1 - S^{\pm}) \quad (27)$$

coincides, except for the double sign in $S^{\pm}$, with the corresponding stationary expression.[19] Combining eqs 24−26 shows that

$$\delta\tilde{C}_s^{*\pm} = (M^{\pm} \pm S^{\pm})\delta\tilde{n}^*(a) \quad (28)$$

so that the frequency dependence of $\delta C_s^{*\pm}$ is solely determined by $\delta\tilde{n}^*(a)$.

Using these results, eq 21 finally transforms into

$$a\nabla_r\delta\tilde{\mu}^{*\pm}|_a = \frac{2G_0^{\pm}}{z^{\mp}Na}[\delta\tilde{n}^*(a) \pm z^{\pm}\delta\tilde{\varphi}^*(a)] + \frac{2D_s^{\pm}C_{s0}^{\pm}}{D^{\pm}z^{\mp}Na}[M^{*\pm}\delta\tilde{n}^*(a) \pm z^{\pm}\delta\tilde{\varphi}^*(a)] + \frac{3m^{\pm}}{\kappa a}\frac{z^{\pm}z^{\pm}}{z^{\mp}}[I_{eo}^{\pm}\delta\tilde{\varphi}^*(a) + I_{co}^{\pm}\delta\tilde{n}^*(a)] + \frac{i\omega a}{z^{\mp}ND^{\pm}}\int_a^\infty(\delta C^{*\pm} - z^{\mp}N\delta\tilde{n}^*)\,dr \quad (29)$$

where

$$m^{\pm} = \frac{2\varepsilon_e}{3\eta_e D^{\pm}}\left(\frac{kT}{z^{\pm}e}\right)^2$$

LOW FREQUENCY SOLUTION

The last addend in eq 29 is classically neglected because it is proportional to the frequency, so that it should be small in the range of the low frequency dielectric dispersion.[18] The same argument should also apply to the frequency dependent part of $M^{*\pm}$, eq 26, which so reduces to $M^{\pm}$, eq 27. Using eqs

dx.doi.org/10.1021/jp3075404 | J. Phys. Chem. B 2012, 116, 13538−13553

9, 10, and 14 and factoring with respect to the coefficients leads to the final equation system:

$$K_c^*[(1 \pm z^{\pm}\Delta)(r^{\pm} + f^*) - u^{\pm}] \pm z^{\pm}K_d^*(r^{\pm} + 2) = \pm z^{\pm}(r^{\pm} - 1) \quad (30)$$

where

$$r^{\pm} = R^{\pm} + R_s^{\pm} \quad (31)$$

$$u^{\pm} = U^{\pm} + (1 - M^{\pm})R_s^{\pm}$$

$$f^* = 2 + \frac{\xi^*\kappa^2 a^2}{1 + \sqrt{\xi^*}\kappa a} = 2 + 2h^*$$

while the coefficients

$$R^{\pm} = \frac{2G_0^{\pm}}{z^{\mp}Na} \pm \frac{3m^{\pm}z^{\pm}}{z^{\mp}\kappa a}I_{eo}^{\pm} \quad (32)$$

$$R_s^{\pm} = \frac{2D_s^{\pm}C_{s0}^{\pm}}{D^{\pm}z^{\mp}Na} \quad (33)$$

$$U^{\pm} = \frac{3m^{\pm}z^{\pm}}{z^{\mp}\kappa a}(\pm I_{eo}^{\pm} - z^{\pm}I_{co}^{\pm})$$

are the same as when there is no stagnant layer.[17] Note that eq 30 has exactly the same form as eq 35 in ref 17 with $r^{\pm}$ and $u^{\pm}$ replacing $R^{\pm}$ and $U^{\pm}$, respectively. This similarity makes it possible to write down the solution in the same form as eqs 32 and 33 in ref 17:

$$K_c^* = \frac{3\frac{2z^+z^-}{z^+ + z^-}\frac{r^+ - r^-}{2B}}{1 + h^*A/B} \quad (34)$$

$$K_d^* = K_{d\infty} - K_c^*H \quad (35)$$

where $K_{d\infty}$, H, A, and B are real frequency independent coefficients:

$$K_{d\infty} = \lim_{\omega\to\infty} K_d = \frac{\frac{z^+D^+r^+ + z^-D^-r^-}{z^+D^+ + z^-D^-} - 1}{\frac{z^+D^+r^+ + z^-D^-r^-}{z^+D^+ + z^-D^-} + 2} \quad (36)$$

$$H = \frac{D_{ef}(r^+ - r^-) - D^+u^+ + D^-u^-}{z^+D^+(r^+ + 2) + z^-D^-(r^- + 2)}$$

$$A = 2\frac{z^+D^+r^+ + z^-D^-r^-}{z^+D^+ + z^-D^-} + 4 \quad (37)$$

$$B = (r^+ + 2)(r^- + 2) - \frac{z^+(r^+ + 2)u^- + z^-(r^- + 2)u^+}{z^+ + z^-}$$

Note that the coefficients $K_{d\infty}$, H, and A have been written in a simpler form than in ref 17 by using the expressions for Δ and D_{ef}, and noting that $D^+U^+ = D^-U^-$.[18]

In the stationary limit, $\omega = 0$, eqs 34 and 35 reduce to

$$K_c(0) = \frac{3z^+z^-(r^+ - r^-)}{z^+(r^+ + 2)(r^- + 2 - u^-) + z^-(r^- + 2)(r^+ + 2 - u^+)}$$

$$K_d(0) = \frac{z^+(r^+ - 1)(r^- + 2 - u^-) + z^-(r^- - 1)(r^+ + 2 - u^+) - 3z^+z^-(r^+ - r^-)\Delta}{z^+(r^+ + 2)(r^- + 2 - u^-) + z^-(r^- + 2)(r^+ + 2 - u^+)} \quad (38)$$

As expected,[17] $K_c(0)$ coincides with the stationary expression, eq 38 in ref 19:

$$K_c(0) = K_c$$

while $K_d(0)$ does not coincide with the stationary result, eq 37 in ref 19, but rather satisfies

$$K_d(0) = K_d - K_c(0)\Delta$$

The form of eq 36 makes it possible to relate the coefficients $r^{\pm}$ to the total (diffuse plus stagnant layer) surface conductivity λ:[17]

$$\frac{z^+D^+r^+ + z^-D^-r^-}{z^+D^+ + z^-D^-} = \frac{2\lambda}{aK_e} \quad (39)$$

where K_e is the bulk conductivity of the electrolyte solution

$$K_e = \frac{(z^+e)^2D^+z^-N + (z^-e)^2D^-z^+N}{kT} = \frac{z^+D^+ + z^-D^-}{z^+ + z^-}\kappa^2\varepsilon_e \quad (40)$$

These results, together with eqs 31−33, lead to the final expression

$$\lambda = \frac{(z^+e)^2D^+G_0^+(1 + 3m^+) + (z^-e)^2D^-G_0^-(1 + 3m^-)}{kT} + \frac{(z^+e)^2D_s^+C_{s0}^+ + (z^-e)^2D_s^-C_{s0}^-}{kT} \quad (41)$$

where the first addend coincides with the Bikerman result for the surface conductivity of the diffuse double layer,[20] while the second one corresponds to the stagnant layer surface conductivity.

Figure 1 represents the total surface conductivity as a function of the $\tilde{\zeta}$ potential and its dependence on the counterion and co-ion valences and on the stagnant layer parameters. This and all the following figures use the system parameters given in Table 1, which were taken from ref 10 in order to be able to visually compare the obtained results with numerical data from that reference.

For $z^+ = z^- = 1$, they roughly correspond to a suspension of 100 nm particles in an aqueous 10 mM/L KCl solution. The actual electrolyte concentration was calculated in all cases from the reciprocal Debye length, eq 3, and the condition $\kappa a = 30$. Note that a constant Debye length also implies a constant bulk conductivity when the counterion and co-ion diffusion coefficients have the same value, eq 40. The maximum adsorbed ion concentrations $N_s^{\pm}$ correspond to a maximum surface charge density of ± 0.8 C m^{-2} for $z^+ = z^- = 1$. The last two columns in Table 1 determine the dissociation constant values written as $K_s^{\pm} = 1000N_A10^{-pK^{\pm}}m^{-3}$ so that for co-ions $K_s^+ = 6.022 \times 10^{25}$ m^{-3}, while for counterions 6.022×10^{24} m$^{-3} \le K_s^- \le 6.022 \times 10^{28}$ m^{-3}.

Figure 1a shows the rapid increase of the diffuse double layer conductivity with the surface potential, which is mainly due to the increase of the counterion population in this layer. The very strong dependence with the counterion valence is due to the increase of the factor multiplying the $\tilde{\zeta}$ potential in the

dx.doi.org/10.1021/jp3075404 | J. Phys. Chem. B 2012, 116, 13538−13553

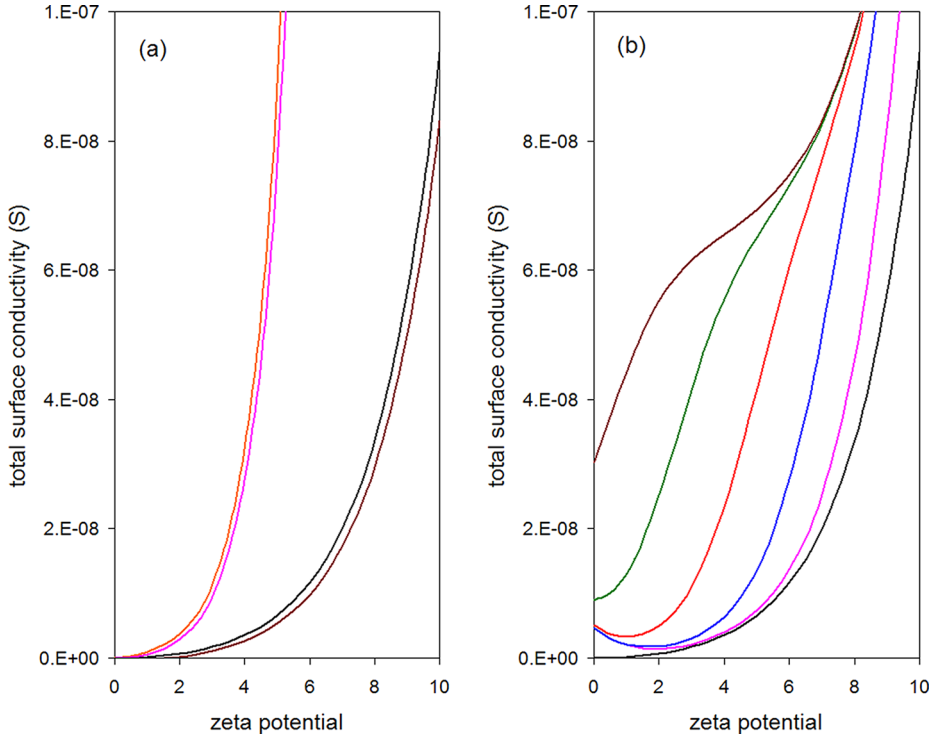

Figure 1. Total surface conductivity as a function of the $\tilde{\zeta}$ potential and its dependence on (a) the counterion and co-ion valences and (b) the stagnant layer parameters. (a) No stagnant layer; $z^+ = z^- = 1$ (black), $z^+ = 2z^- = 2$ (brown), $2z^+ = z^- = 2$ (orange), and $z^+ = z^- = 2$ (magenta) lines. (b) $z^+ = z^- = 1$; no stagnant layer (black), stagnant layer with $pK^+ = 1$ and $pK^- = -2$ (magenta), $= -1$ (blue), $= 0$ (red), $= 1$ (green), and $= 2$ (brown) lines. Remaining system parameters are given in Table 1.

Table 1. System Parameters Used in All the Figures except When Stated Otherwise

$T = 298.16$ K	$a = 10^{-7}$ m	$pK^+ = 1$	$pK^- = -2$
$\varepsilon_e = 78.54\varepsilon_0$	$\tilde{\zeta} = 4$	$pK^+ = 1$	$pK^- = -1$
$\eta_e = 8.904 \times 10^{-4}$ N s m^{-2}	$\kappa a = 30$	$pK^+ = 1$	$pK^- = 0$
$D^{\pm} = D_s^{\pm} = 2 \times 10^{-9}$ m^2 s^{-1}	$K_e = 0.1501$ S m^{-1}	$pK^+ = 1$	$pK^- = 1$
$z^+ = z^- = 1$	$N_s^{\pm} = 4.994 \times 10^{18}$ m^{-2}	$pK^+ = 1$	$pK^- = 2$

exponential function of eqs 16−18 (for high $\tilde{\zeta}$, G_0^{11-} and G_0^{21-} become proportional to $e^{z\tilde{\zeta}/2}$ while G_0^{12-} and G_0^{22-} increase as $e^{z\tilde{\zeta}}$). The weak dependence of the surface conductivity with the co-ion valence is mainly due to the dependence of the bulk counterion concentration on the co-ion valence at constant Debye length: for univalent counterions, an increase of the co-ion valence from 1 to 2 decreases the counterion concentration by a factor of 2/3, while, for divalent counterions, the corresponding factor is 3/4, eq 3.

Figure 1b shows that, for low $\tilde{\zeta}$ potentials, the total surface conductivity strongly increases with the pK^- value, which determines the counterion population in the stagnant layer. Note that, in general, the surface conductivity does not reduce to zero for $\tilde{\zeta} = 0$ and that its minimum is not necessarily attained for $\tilde{\zeta} = 0$. This occurs because for the magenta, blue, and red lines $pK^+ > pK^-$, so that the population of co-ions in the stagnant layer surpasses that of counterions for $\tilde{\zeta} = 0$. For the green line, these populations coincide (the corresponding minimum is located at $\tilde{\zeta} = 0$), while, for the brown line, the population of counterions surpasses that of co-ions so that the corresponding minimum occurs for a negative value of the $\tilde{\zeta}$ potential (outside the figure). Finally, for high values of the $\tilde{\zeta}$ potential, the counterion population in the stagnant layer saturates so that the increase of the total surface conductivity with the $\tilde{\zeta}$ potential is only due to the diffuse double layer contribution, first addend in the right-hand side of eq 41 (black line).

Figures 2 and 3 represent the real part of the concentration and dipole coefficient spectra, eqs 34 and 35, and their dependences on the counterion and co-ion valences and on the stagnant layer parameters.

Figures 2a and 3a show the expected strong increase of the concentration and dipole coefficients with the counterion valence. However, they also show a strong dependence on the co-ion valence, even though there are almost no co-ions in the diffuse double layer. Moreover, the dependences of the dipole and the concentration coefficients on the co-ion valences are qualitatively different: extreme $\mathrm{Re}(K_d^*)$ values correspond to different counterion and co-ion valences, while extreme $\mathrm{Re}(K_c^*)$ values are attained when counterion and co-ion valences are the same. The reason for this difference is that the dipolar coefficient is determined by the ratio of the double layer surface conductivity and the bulk conductivity of the electrolyte solution. On the contrary, the concentration coefficient depends on the ratio of the counterion transfer numbers in the double layer and in the electrolyte solution. Since at constant κ the electrolyte solution conductivity is also constant, eq 40 with $D^+ = D^-$, the qualitative dependence of $\mathrm{Re}(K_d^*)$ with the counterion and co-ion valences, Figure 2a, coincides with that of the surface conductivity, Figure 1a.

As for the concentration coefficient, consider that the counterion valence is one while the co-ion valence changes to two. The modulus of $\mathrm{Re}(K_c^*)$ should increase because the bulk conductivity part due to counterions, last addend in the second equality in eq 40, decreases (by a factor 2/3). Likewise, starting with divalent ions and lowering the co-ion valence to one, the bulk conductivity part due to counterions increases (by a factor of 4/3) so that the modulus of $\mathrm{Re}(K_c^*)$ should decrease, in agreement with Figure 2a.

dx.doi.org/10.1021/jp3075404 | J. Phys. Chem. B 2012, 116, 13538−13553

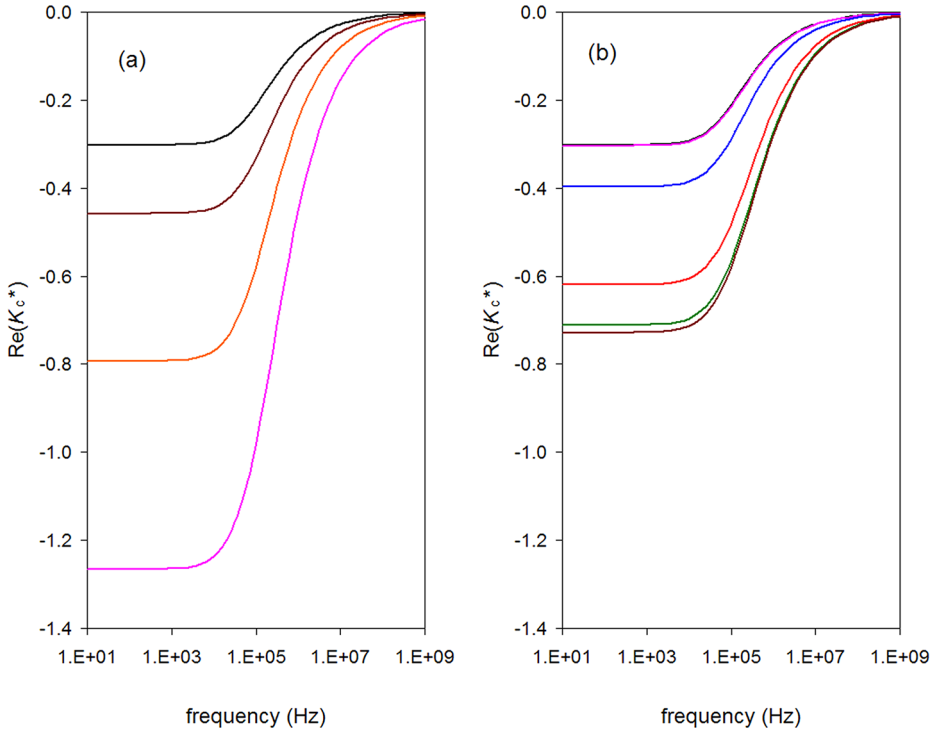

Figure 2. Real part of the concentration coefficient spectra, eq 34, and their dependences on (a) the counterion and co-ion valences and (b) the stagnant layer parameters. (a) No stagnant layer; $z^+ = z^- = 1$ (black), $z^+ = 2z^- = 2$ (brown), $2z^+ = z^- = 2$ (orange), and $z^+ = z^- = 2$ (magenta) lines. (b) $z^+ = z^- = 1$; no stagnant layer (black), stagnant layer with $pK^+ = 1$ and $pK^- = -2$ (magenta), = −1 (blue), = 0 (red), = 1 (green), and = 2 (brown) lines. Remaining system parameters are given in Table 1.

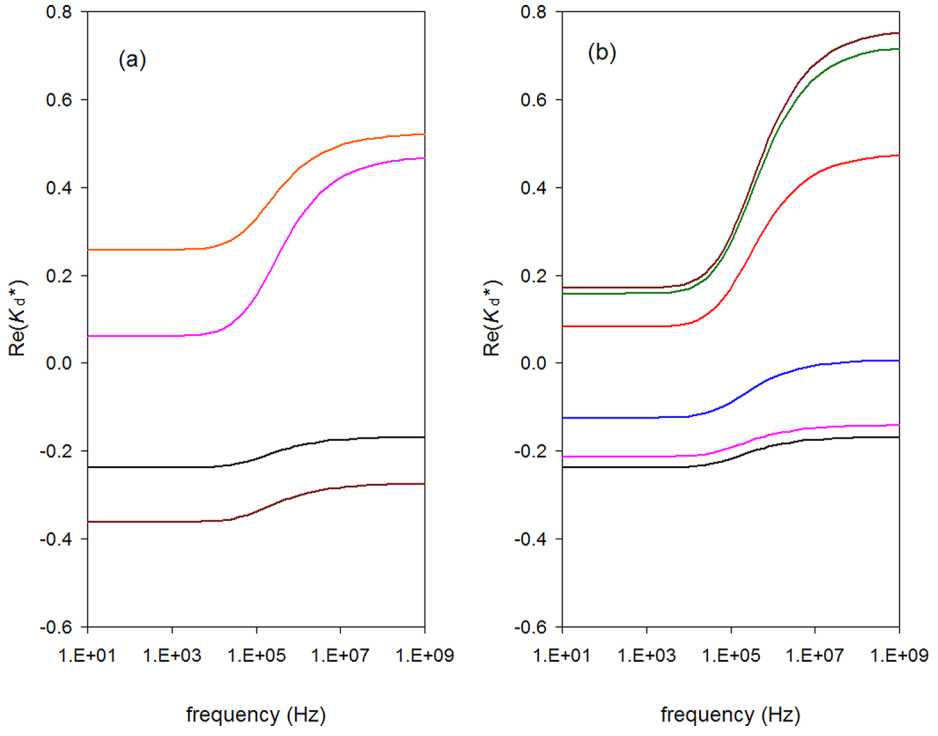

Figure 3. Real part of the dipole coefficient spectra, eq 35, and their dependences on (a) the counterion and co-ion valences and (b) the stagnant layer parameters. (a) No stagnant layer; $z^+ = z^- = 1$ (black), $z^+ = 2z^- = 2$ (brown), $2z^+ = z^- = 2$ (orange), and $z^+ = z^- = 2$ (magenta) lines. (b) $z^+ = z^- = 1$; no stagnant layer (black), stagnant layer with $pK^+ = 1$ and $pK^- = -2$ (magenta), = −1 (blue), = 0 (red), = 1 (green), and = 2 (brown) lines. Remaining system parameters are given in Table 1.

Figures 2b and 3b show the expected monotonous increase of the concentration and dipole coefficients with the counterion population in the stagnant layer.[19] None of the above-mentioned complications appear in this case because the considered stagnant layer conductivity changes occur without modifying any of the bulk electrolyte solution properties.

dx.doi.org/10.1021/jp3075404 | J. Phys. Chem. B 2012, 116, 13538−13553

As for the frequency dependence, the concentration coefficient, Figure 2, has the expected behavior: a broad relaxation tending to zero at high frequencies. The dipole coefficient behavior, Figure 3, also shows the low frequency relaxation but lacks the expected high frequency Maxwell−Wagner−O'Konski relaxation, which was suppressed from the model when the terms proportional to the frequency in eq 29 were set to zero.

HIGH FREQUENCY EXTENSION

As shown in ref 18, the validity of the obtained expression for the dipole coefficient can be extended to higher frequencies (including the Maxwell−Wagner−O'Konski dispersion) by taking into account in eq 29 the presence of the terms that are proportional to the frequency. Equation 29 is first written as

$$K_c^*[D_{ef}(r^\pm + f^*) - D^\pm u^{*\pm}] \pm z^\pm D^\pm K_d^*(r^\pm + 2) = \pm z^\pm D^\pm (r^\pm - 1) - \frac{i\omega kT}{z^+ z^- NeE\cos\theta}\int_a^\infty (z^\pm \delta C^{*\pm} - z^+ z^- N\delta\tilde{n}^*)\,dr$$

where

$$u^{*\pm} = U^\pm + (1 - M^{*\pm})R_s^\pm$$

Subtracting the second (lower sign) equation from the first (upper sign) and solving for K_d^* gives

$$K_d^* = K_{d\infty} - K_c^* H^* - \frac{i\omega}{K_e(A/2)E\cos\theta}\int_a^\infty (z^+ e\delta C^{*+} - z^- e\delta C^{*-})\,dr$$

where

$$H^* = \frac{D_{ef}(r^+ - r^-) - D^+ u^{*+} + D^- u^{*-}}{z^+ D^+ (r^+ + 2) + z^- D^- (r^- + 2)}$$

This result is similar to the low frequency eq 35 except for the frequency dependence of H^* and for the presence of the last addend, in which the integral represents the field-induced surface charge density $\delta\rho^*$ located outside the stagnant layer. This charge density can be calculated considering the discontinuity of the radial component of the field-induced displacement:[18]

$$-\varepsilon_e\left.\frac{\partial\delta\Phi^*}{\partial r}\right|_a + \varepsilon_i\left.\frac{\partial\delta\Phi_i^*}{\partial r}\right|_a = \int_a^\infty (z^+ e\,\delta C^{*+} - z^- e\,\delta C^{*-})\,dr - \frac{\kappa^2\varepsilon_e kT}{e}\int_a^\infty \delta\tilde{\rho}^*\,dr + [z^+ eC_{s0}^+(M^+ + S^+) - z^- eC_{s0}^-(M^- - S^-)]\delta\tilde{n}^*(a) \quad (42)$$

In this expression, Φ_i^* is the field-induced potential inside the particle, the second integral represents the surface charge density located outside the diffuse double layer, $\delta\tilde{\rho}^* = e\delta\rho^*/(\kappa^2\varepsilon_e kT)$, and the last addend corresponds to the field-induced surface charge density of the stagnant layer. The presence of this last addend, which was written using eq 28, is the only difference between eq 42 and eq 32 in ref 18. Following precisely the same procedure as in that reference leads to the following expression for the dipole coefficient:

$$K_d^* = \frac{\varepsilon_i - \varepsilon_e}{\varepsilon_i + 2\varepsilon_e} + \frac{K_{d\infty} - \frac{\varepsilon_i - \varepsilon_e}{\varepsilon_i + 2\varepsilon_e}}{1 + i\omega\frac{\varepsilon_i + 2\varepsilon_e}{K_e A/2}} - \frac{K_c^* H^*}{1 + i\omega\frac{\varepsilon_i + 2\varepsilon_e}{K_e A/2}} + i\omega\frac{K_c^* a}{K_e A/2}\frac{e}{kT}\frac{z^+ eC_{s0}^+(M^+ + S^+) - z^- eC_{s0}^-(M^- - S^-)}{1 + i\omega\frac{\varepsilon_i + 2\varepsilon_e}{K_e A/2}} \quad (43)$$

while eq 34 for the concentration coefficient remains unaltered.

In the high frequency limit, the concentration coefficient tends to zero so that the dipolar coefficient reduces to the first two addends in the right-hand side of eq 43, which can be written using eqs 36, 37, and 39 as

$$K_d^* \sim \frac{\varepsilon_i - \varepsilon_e}{\varepsilon_i + 2\varepsilon_e} + \frac{\frac{2\lambda/a - K_e}{2\lambda/a + 2K_e} - \frac{\varepsilon_i - \varepsilon_e}{\varepsilon_i + 2\varepsilon_e}}{1 + i\omega\frac{\varepsilon_i + 2\varepsilon_e}{2\lambda/a + 2K_e}} \quad (44)$$

This expression coincides with the classical Maxwell−Wagner−O'Konski relaxation[21−23] written in terms of the total surface conductivity.

Figures 4 and 5 represent the real part of the dipole coefficient spectra, eq 43, and their dependences on the counterion and co-ion valences and on the stagnant layer parameters. Both clearly show the high frequency relaxation, absent in Figure 3, the increase of the relaxation frequency with the total surface conductivity, and the convergence of all the plotted lines to a single high frequency limiting value that only depends on the particle and electrolyte solution permittivities, eq 44.

The dotted lines in Figure 4 represent numerical results obtained with the Hill−Saville−Russel program,[24] using precisely the same system parameters. As can be seen, the agreement is extremely good for univalent counterions and acceptable for the two divalent cases. Moreover, the agreement at high frequencies is excellent for all the considered cases. The deviations observed at low frequencies for divalent counterions have their origin in a well-known feature of the original theory: its agreement with numerical results worsens with increasing $\tilde{\zeta}$ potential values[25] (it improves however with increasing κa). While this behavior is still not well understood, it is most likely related to the value of the surface conductivity that rapidly increases with the $\tilde{\zeta}$ potential, Figure 1a. This figure also shows that, for $\tilde{\zeta} = 4$, which is the value used in Figure 4, the surface conductivity for divalent counterions is almost an order of magnitude greater than for univalent ones.

As for the excellent agreement observed at high frequencies, it occurs because under these conditions the analytical treatment only differs from the numerical one by the use of the thin double layer approximation and the neglect of all inertial effects.

The empty diamonds in Figure 5 represent numerical results copied from the upper part of Figure 10 in ref 10, while the solid diamonds on the vertical axis correspond to numerical results obtained with the Mangelsdorf−White DC program.[8] As can be seen, there is no agreement between the AC and DC numerical results, except for the black and brown diamonds, which seems to indicate that lines B, C, and D in Figure 10 in ref 10 (magenta, blue, and red empty diamonds) do not correspond to the parameter values appearing in the captions of that figure. A comparison of our results with the DC numerical data and the qualitative frequency dependence of the AC numerical values suggests a good agreement for low and moderate stagnant

dx.doi.org/10.1021/jp3075404 | J. Phys. Chem. B 2012, 116, 13538−13553

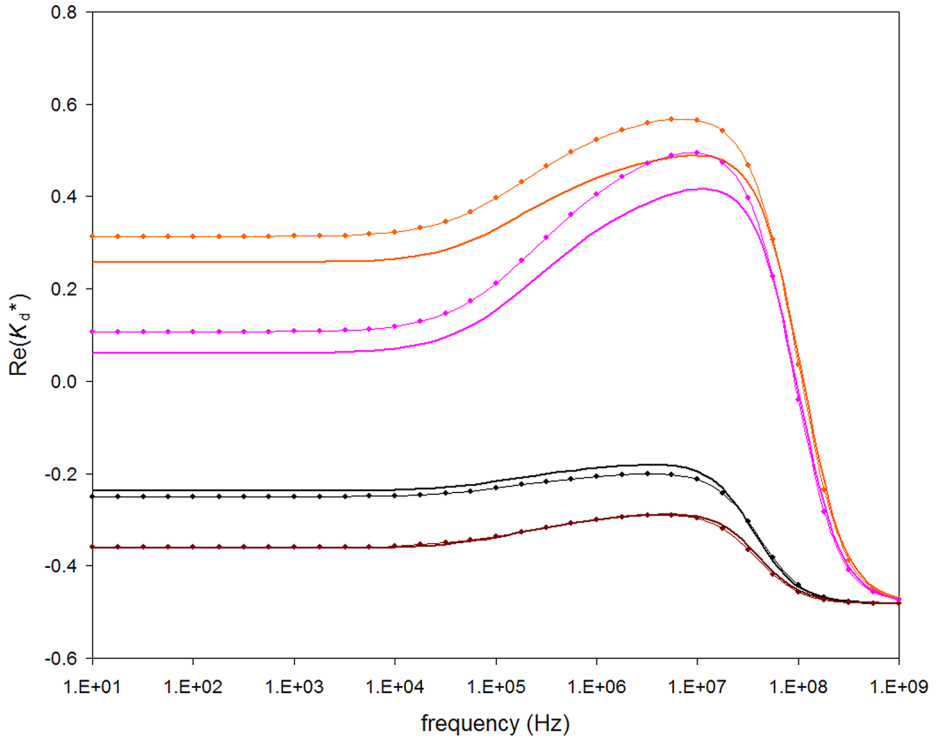

Figure 4. Real part of the dipole coefficient spectra, eq 43, and their dependences on the counterion and co-ion valences, considering that there is no stagnant layer. $z^+ = z^- = 1$ (black), $z^+ = 2z^- = 2$ (brown), $2z^+ = z^- = 2$ (orange), and $z^+ = z^- = 2$ (magenta) lines. Dotted lines: numerical results obtained with the Hill–Saville–Russel program.[24] Remaining system parameters are given in Table 1.

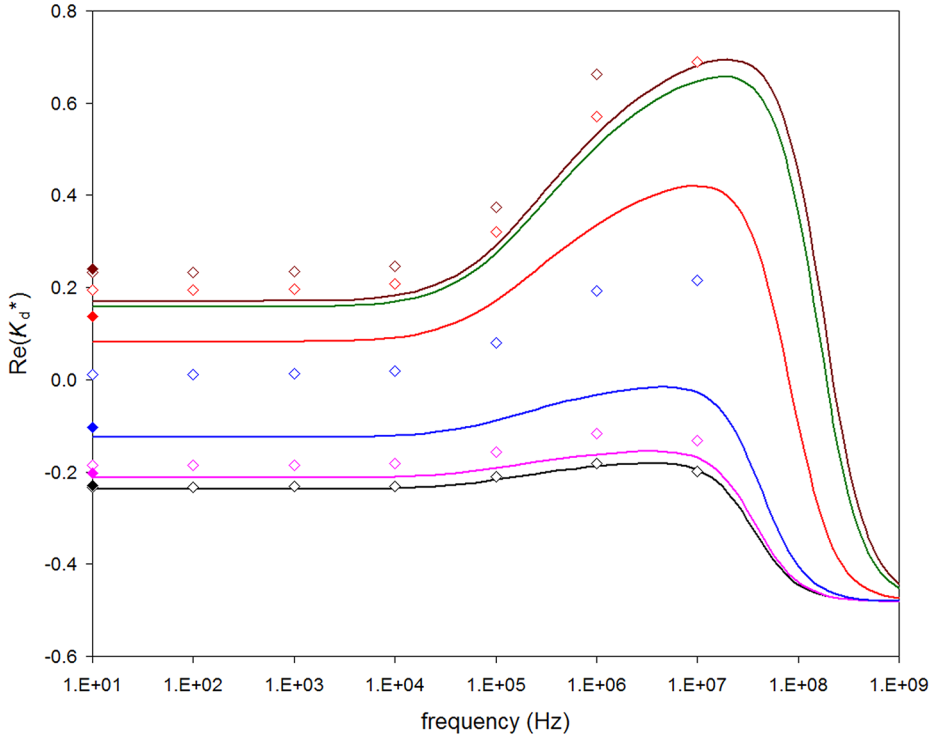

Figure 5. Real part of the dipole coefficient spectra, eq 43, and their dependences on the stagnant layer parameters, considering that $z^+ = z^- = 1$. No stagnant layer (black), stagnant layer with $pK^+ = 1$ and $pK^- = -2$ (magenta), $= -1$ (blue), $= 0$ (red), $= 1$ (green), and $= 2$ (brown) lines. Empty diamonds: numerical results copied from the upper part of Figure 10 in ref 10; see text. Solid diamonds on vertical axis: numerical results obtained with the Mangelsdorf–White DC program.[8] Remaining system parameters are given in Table 1.

layer conductivities, which worsens for the highest conductivity values. The reason for this behavior is most certainly the same as that discussed after Figure 4. In order to provide a more precise comparison with numerical data, we tried to use the Mangelsdorf–White AC program,[10] but unfortunately it fails to execute on current hardware.

dx.doi.org/10.1021/jp3075404 | J. Phys. Chem. B 2012, 116, 13538–13553

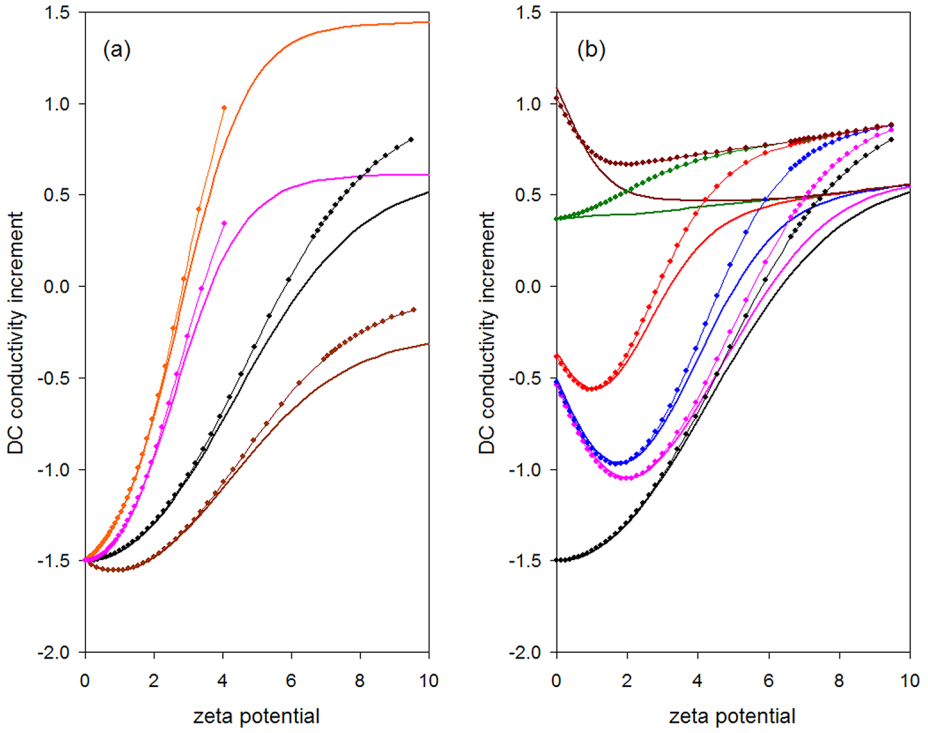

Figure 6. DC conductivity increment, eqs 38 and 45, as a function of the $\tilde{\zeta}$ potential and its dependence on (a) the counterion and co-ion valences and (b) the stagnant layer parameters. (a) No stagnant layer; $z^+ = z^- = 1$ (black), $z^+ = 2z^- = 2$ (brown), $2z^+ = z^- = 2$ (orange), and $z^+ = z^- = 2$ (magenta) lines. (b) $z^+ = z^- = 1$; no stagnant layer (black), stagnant layer with $pK^+ = 1$ and $pK^- = -2$ (magenta), $= -1$ (blue), $= 0$ (red), $= 1$ (green), and $= 2$ (brown) lines. Dotted lines: numerical results obtained with the Mangelsdorf–White DC program.[8] Remaining system parameters are given in Table 1.

COMPLEX CONDUCTIVITY INCREMENT

The complex conductivity increment of a dilute suspension has the general form

$$\frac{K^* - K_e^*}{\phi} = 3K_e^* K_d^*$$

where ϕ is the volume fraction of particles in the suspension and

$$K^* = K(\omega) + i\omega\varepsilon(\omega)$$

$$K_e^* = K_e + i\omega\varepsilon_e$$

are the complex conductivities of the suspension and of the electrolyte solution, respectively.

Separating the real and imaginary parts leads to the following expressions for the conductivity and permittivity increments:

$$\frac{K(\omega) - K_e}{\phi K_e} = 3[\mathrm{Re}(K_d^*) - \omega\tau_e\,\mathrm{Im}(K_d^*)] \quad (45)$$

$$\frac{\varepsilon(\omega) - \varepsilon_e}{\phi\varepsilon_e} = 3\left[\mathrm{Re}(K_d^*) + \frac{\mathrm{Im}(K_d^*)}{\omega\tau_e}\right] \quad (46)$$

where

$$\tau_e = \varepsilon_e/K_e$$

is the electrolyte solution relaxation time.

Figure 6 represents the DC conductivity increment as a function of the $\tilde{\zeta}$ potential and its dependence on the counterion and co-ion valences and on the stagnant layer parameters. The dotted lines represent numerical results obtained with the Mangelsdorf–White DC program,[8] using precisely the same system parameters. As can be seen, the agreement is quite good, at least for low and moderate $\tilde{\zeta}$ potentials. As already noted, the deviations observed for high $\tilde{\zeta}$ potentials appear to originate in the classical (no stagnant layer) formulation of the theory, as can be seen comparing the full and dotted black lines. Moreover, these deviations become stronger for divalent counterions and for increasing pK^- values that lead to higher surface conductivity values at any given $\tilde{\zeta}$ potential, Figure 1.

Figure 6a shows that the stationary dipolar coefficient (1/3 of the DC conductivity increment, eq 45) for symmetric univalent and divalent electrolytes converges to a single value of ~1/4 for high $\tilde{\zeta}$ potentials, while it tends to ~0 for univalent counterions and divalent co-ions, and to ~1/2 for divalent counterions and univalent co-ions.[16] Note also that the prediction made in that reference that the dipolar coefficient should attain values lower than −1/2 for univalent counterions and divalent co-ions is well confirmed by the numerical data.

Figures 7–10 represent the conductivity and permittivity increment spectra, and their dependences on the counterion and co-ion valences and on the stagnant layer parameters. In Figures 9 and 10, the whole spectra are plotted over the left vertical axis and just their high frequency part over the right ordinate.

The dotted lines in Figures 7 and 9 represent numerical results obtained with the Hill–Saville–Russel program,[24] using precisely the same system parameters. As can be seen, the agreement at low frequencies is very good for univalent counterions and acceptable for divalent ones. At high frequencies, however, the agreement is excellent for all the considered cases.

Figures 9 and 10 show the extreme sensitivity of the high frequency permittivity behavior on the surface conductivity, in agreement with eq 44: both the dispersion amplitude and characteristic frequency increase with the total surface conductivity. This has a considerable practical importance, since it shows that the high frequency dielectric dispersion

dx.doi.org/10.1021/jp3075404 | J. Phys. Chem. B 2012, 116, 13538–13553

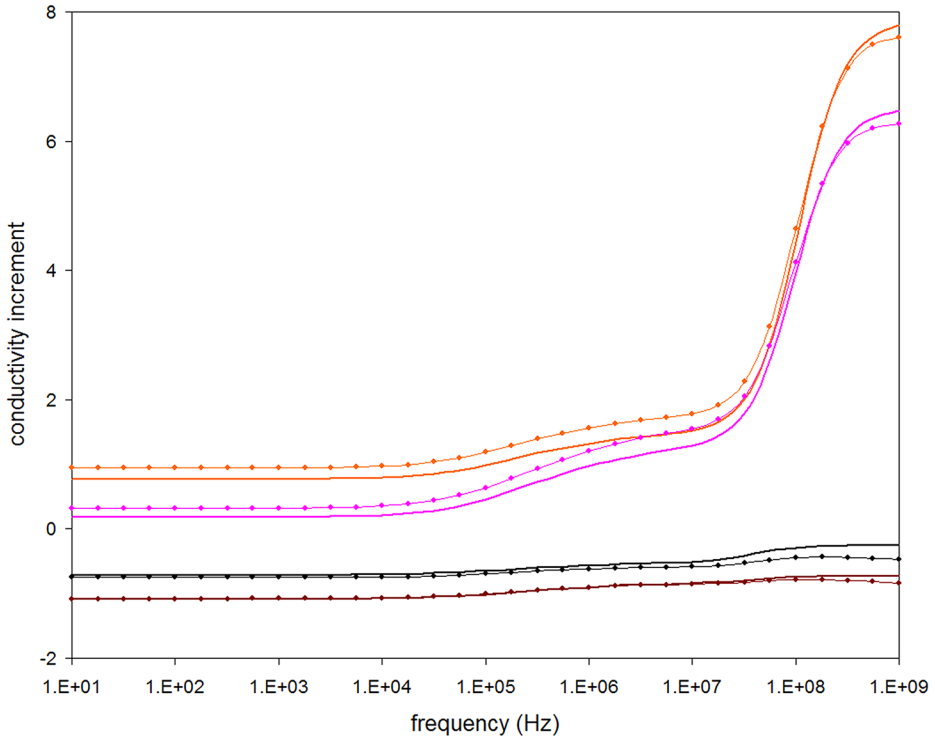

Figure 7. Conductivity increment spectra, eq 45, and their dependences on the counterion and co-ion valences, considering that there is no stagnant layer. $z^+ = z^- = 1$ (black), $z^+ = 2z^- = 2$ (brown), $2z^+ = z^- = 2$ (orange), and $z^+ = z^- = 2$ (magenta) lines. Dotted lines: numerical results obtained with the Hill–Saville–Russel program.[24] Remaining system parameters given in Table 1.

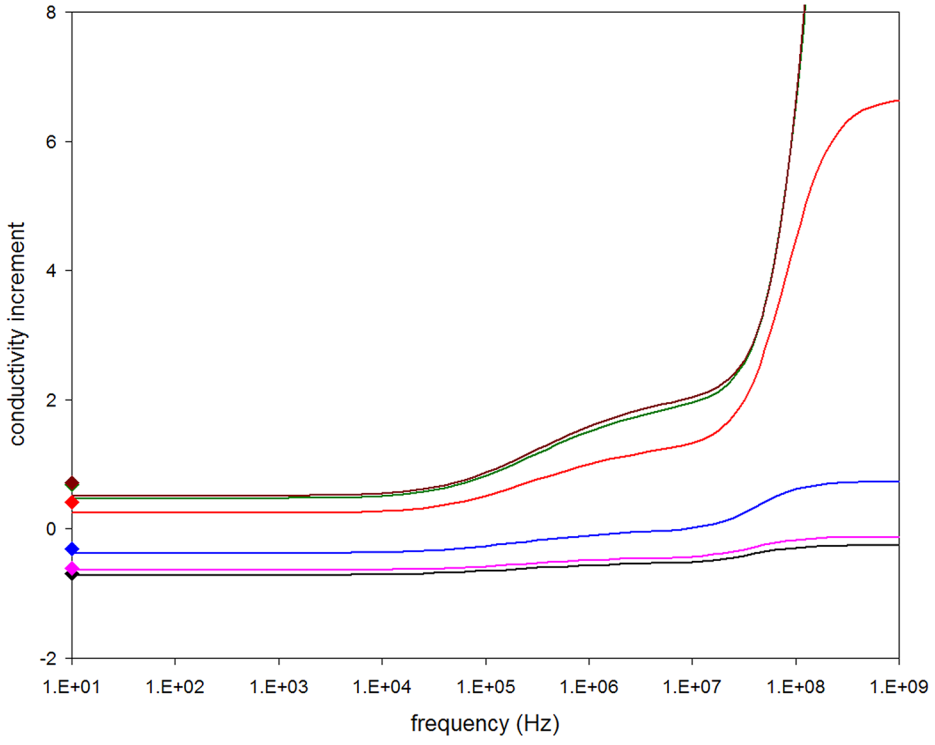

Figure 8. Conductivity increment spectra, eq 45, and their dependences on the stagnant layer parameters, considering that $z^+ = z^- = 1$. No stagnant layer (black), stagnant layer with $pK^+ = 1$ and $pK^- = -2$ (magenta), = −1 (blue), = 0 (red), = 1 (green), and = 2 (brown) lines. Solid diamonds on vertical axis: numerical results obtained with the Mangelsdorf–White DC program.[8] Remaining system parameters given in Table 1.

data constitutes the most direct source of information for the determination of the total surface conductivity.

Conductivity and permittivity increment spectra were not calculated in ref 10 so that a visual comparison of the obtained results with numerical data from that reference is impossible. However, Figure 8 includes numerical values obtained with the Mangelsdorf–White DC program,[8] using precisely the same system parameters (solid diamonds on the vertical axis).

dx.doi.org/10.1021/jp3075404 | J. Phys. Chem. B 2012, 116, 13538–13553

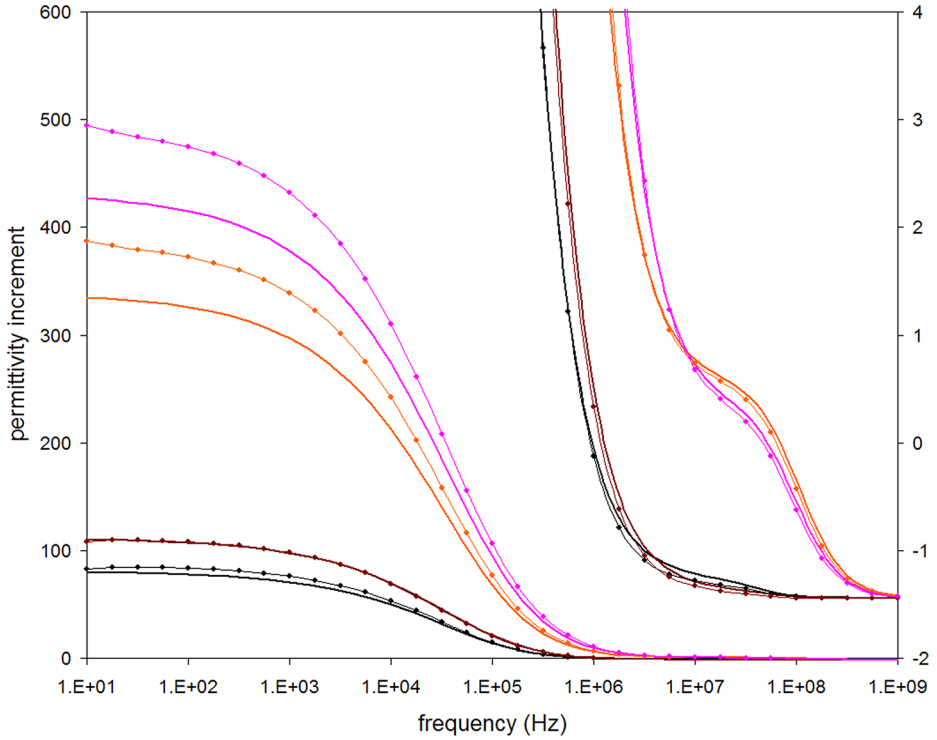

Figure 9. Permittivity increment spectra, eq 46, and their dependences on the counterion and co-ion valences, considering that there is no stagnant layer. The right ordinate corresponds to the high frequency part of the spectra. $z^+ = z^- = 1$ (black), $z^+ = 2z^- = 2$ (brown), $2z^+ = z^- = 2$ (orange), and $z^+ = z^- = 2$ (magenta) lines. Dotted lines: numerical results obtained with the Hill–Saville–Russel program.[24] Remaining system parameters are given in Table 1.

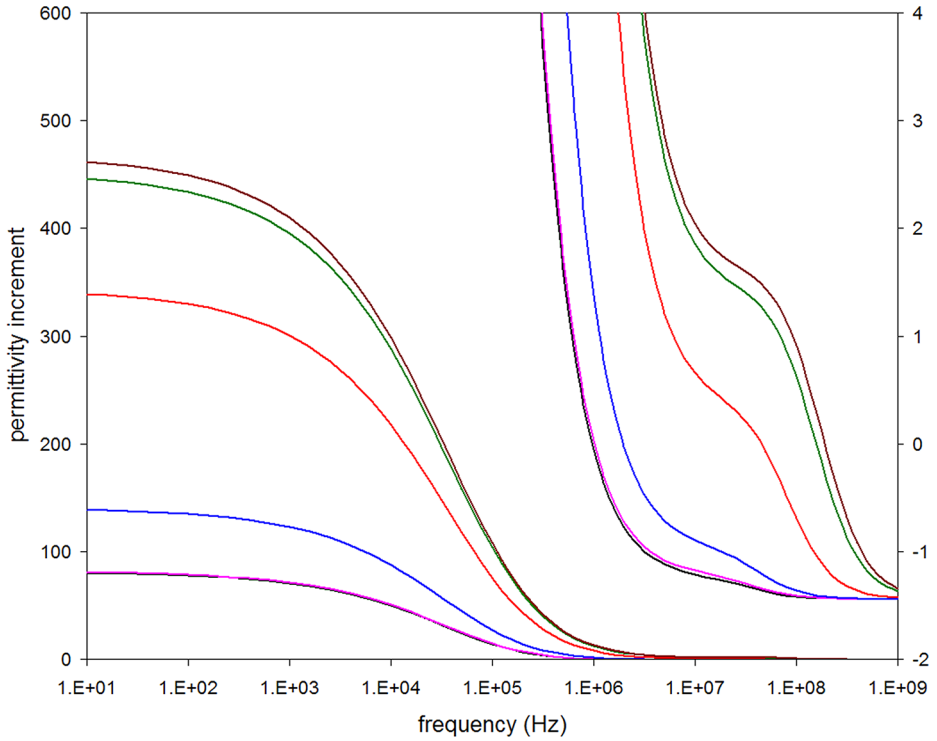

Figure 10. Permittivity increment spectra, eq 46, and their dependences on the stagnant layer parameters, considering that $z^+ = z^- = 1$. The right ordinate corresponds to the high frequency part of the spectra. No stagnant layer (black), stagnant layer with $pK^+ = 1$ and $pK^- = -2$ (magenta), $= -1$ (blue), $= 0$ (red), $= 1$ (green), and $= 2$ (brown) lines. Remaining system parameters are given in Table 1.

A notable feature of Figures 7 and 9 is their qualitatively different dependence on the co-ion valence at low frequencies: extreme conductivity values correspond to different counterion and co-ion valences, while extreme permittivity values are

dx.doi.org/10.1021/jp3075404 | J. Phys. Chem. B 2012, 116, 13538–13553

attained when counterion and co-ion valences are the same, just as in Figures 2a and 3a. The reason for this difference is that, at low frequencies, the conductivity increment is mainly determined by the real part of the dipole coefficient, eq 45, while the imaginary part of K_d^* determines the permittivity increment, eq 46. Also, $\mathrm{Im}(K_d^*)$ has the same qualitative dependence on the co-ion valence at low frequencies as $\mathrm{Re}(K_c^*)$, Figure 2a. Note, finally, that the permittivity increment dependence on the co-ion valence changes to that of the conductivity increment at high frequencies, because then the concentration polarization vanishes, eq 34.

DYNAMIC ELECTROPHORETIC MOBILITY

In the frequency range of the low frequency dielectric dispersion, the electrophoretic mobility can be calculated as in the DC case from the sum of the electroosmotic and of the capillary osmotic velocities on the particle equator just outside the diffuse double layer.[26] However, for frequencies above this dispersion, the dynamic electrophoretic mobility can be written as[27,28]

$$\tilde{u}^* = \tilde{\zeta}(1 - K_d^*)G^*$$

where

$$\tilde{u}^* = \frac{3e\eta_e v_p^*}{2\varepsilon_e kTE}$$

is the dimensionless dynamic electrophoretic mobility, v_p^* is the electrophoretic velocity, and G^* is a factor related to the particle and fluid inertia:

$$G^* = \frac{1 + \sqrt{\frac{i\omega a^2 \rho_e}{\eta_e}}}{1 + \sqrt{\frac{i\omega a^2 \rho_e}{\eta_e}} + \frac{i\omega a^2 \rho_e}{9\eta_e}\left(3 + 2\frac{\rho_i - \rho_e}{\rho_e}\right)}$$

where ρ_e and ρ_i are the mass densities of the electrolyte solution and particle, respectively.

This leads to the following expressions valid over a broad frequency range:[17]

(11) For $z^+ = z^- = z$

$$\tilde{u}^{*11} = \tilde{\zeta}(1 - K_d^{*11} - K_c^{*11}\Delta)G^* + \frac{4}{z^2}\ln\left(\frac{e^{z\tilde{\zeta}/4} + e^{-z\tilde{\zeta}/4}}{2}\right)K_c^{*11} \quad (47)$$

(21) For $z^+ = 2z^- = 2z$

$$\tilde{u}^{*21} = \tilde{\zeta}(1 - K_d^{*21} - K_c^{*21}\Delta)G^* + \frac{3}{z^2}\ln\left[\frac{e^{z\tilde{\zeta}/3}(\sqrt{2 + e^{-z\tilde{\zeta}}} + \sqrt{3e^{-z\tilde{\zeta}}})}{2\sqrt{3}}\right]K_c^{*21} \quad (48)$$

(12) For $2z^+ = z^- = 2z$

$$\tilde{u}^{*12} = \tilde{\zeta}(1 - K_d^{*12} - K_c^{*12}\Delta)G^* + \frac{3}{z^2}\ln\left[\frac{e^{-z\tilde{\zeta}/3}(\sqrt{2 + e^{z\tilde{\zeta}}} + \sqrt{3e^{z\tilde{\zeta}}})}{2\sqrt{3}}\right]K_c^{*12} \quad (49)$$

where K_d^* is given in eq 43.

Figure 11 represents the DC electrophoretic mobility as a function of the $\tilde{\zeta}$ potential and its dependence on the counterion and co-ion valences and on the stagnant layer parameters. The dotted lines correspond to numerical results obtained with the Mangelsdorf–White DC program [8] using precisely the same system parameters. As can be seen, the agreement is quite good over the whole $\tilde{\zeta}$ potential range.

Figure 11a shows that, unlike the conductivity increment, the electrophoretic mobility is essentially independent of the ion valences at low $\tilde{\zeta}$ potentials. On the contrary, for high $\tilde{\zeta}$ values, the electrophoretic mobility strongly decreases when the counterion valence increases.[16]

Figure 11b shows that the electrophoretic mobility only depends on the stagnant layer parameters over a limited $\tilde{\zeta}$ potential range. At $\tilde{\zeta} \approx 8$, the colored lines converge, which occurs when the counterion population in the stagnant layer saturates, Figure 1. Finally, for $\tilde{\zeta} \approx 10$, the counterion population in the diffuse layer surpasses the corresponding population in the stagnant layer so that the colored lines converge to the black line. For divalent counterions (not shown in the figure), the counterion saturation is obviously attained at lower $\tilde{\zeta}$ potentials so that for $\tilde{\zeta} > 7$ the electrophoretic mobility becomes independent of the presence of the stagnant layer.

Figure 12 represents the electrophoretic mobility modulus spectra and their dependence on the counterion and co-ion valences. The dotted lines represent numerical results obtained with the Hill–Saville–Russel program,[24] using precisely the same system parameters. It shows the same qualitative dependence on the ion valences as in Figure 6a, which occurs because the dynamic electrophoretic mobility mainly depends on the dipolar coefficient. This happens because in the considered case, $\Delta \approx 0$, the dependence of eqs 47–49 on the concentration coefficient reduces to the last term, which is small due to the logarithmic function.

Figure 13 represents the electrophoretic mobility modulus spectra and their dependence on the stagnant layer parameters. The empty diamonds represent numerical results copied from the upper part of Figure 9 in ref 10, while the solid diamonds on the vertical axis correspond to numerical results obtained with the Mangelsdorf–White DC program.[8] Just as in the case of Figure 5, there is no agreement between the AC and DC numerical results, except for the black and brown diamonds, so that lines B, C, and D in Figure 9 in ref 10 (magenta, blue, and red empty diamonds) do not seem to correspond to the parameter values appearing in the captions of that figure. A comparison of our results with the DC numerical data and the qualitative frequency dependence of the AC numerical values shows a good agreement for all the considered stagnant layer conductivities.

Finally, an interesting feature of the preceding figures is worth noting. Figures 4 and 5 show that the dipolar coefficient corresponding to divalent ions and no stagnant layer (magenta line in Figure 4) almost exactly coincides with the dipolar coefficient corresponding to univalent ions and a stagnant layer with $pK^+ = 1$ and $pK^- = 0$ (red line in Figure 5). This occurs because the total double layer surface conductivity happens to have practically the same value in these two cases (within 5%, see Figure 1). Because of this, the corresponding conductivity increment lines in Figures 7 and 8 almost coincide, as is also the case for the high frequency permittivity increment (Figures 9 and 10) and high frequency mobility modulus (Figures 12 and 13) spectra. However, the low frequency permittivity increment and low

dx.doi.org/10.1021/jp3075404 | J. Phys. Chem. B 2012, 116, 13538–13553

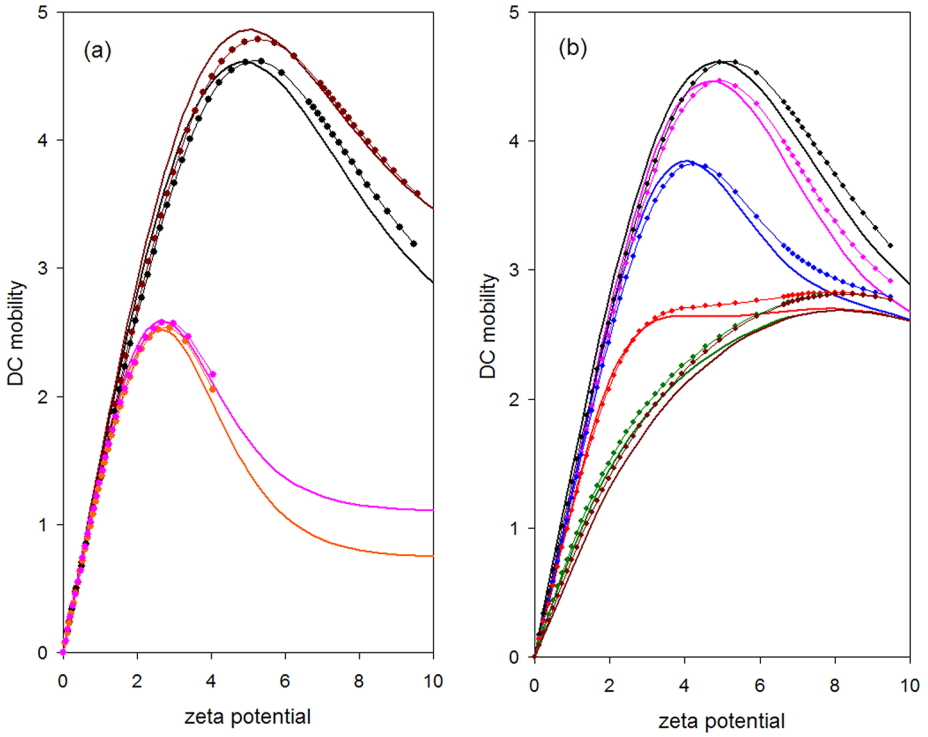

Figure 11. Electrophoretic mobility as a function of the $\tilde{\zeta}$ potential and its dependence on (a) the counterion and co-ion valences and (b) the stagnant layer parameters. (a) No stagnant layer; $z^+ = z^- = 1$ (black), $z^+ = 2z^- = 2$ (brown), $2z^+ = z^- = 2$ (orange), and $z^+ = z^- = 2$ (magenta) lines. (b) $z^+ = z^- = 1$; no stagnant layer (black), stagnant layer with $pK^+ = 1$ and $pK^- = -2$ (magenta), $= -1$ (blue), $= 0$ (red), $= 1$ (green), and $= 2$ (brown) lines. Dotted lines: numerical results obtained with the Mangelsdorf–White DC program.[8] Remaining system parameters are given in Table 1.

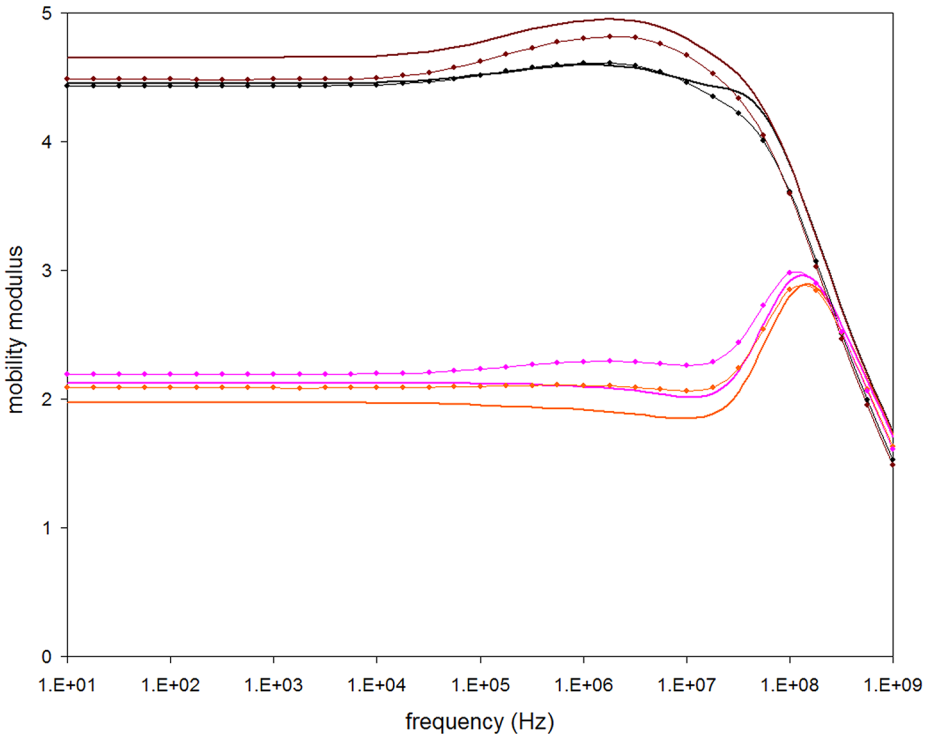

Figure 12. Electrophoretic mobility modulus spectra, eqs 47–49, and their dependence on the counterion and co-ion valences, considering that there is no stagnant layer. $z^+ = z^- = 1$ (black), $z^+ = 2z^- = 2$ (brown), $2z^+ = z^- = 2$ (orange), and $z^+ = z^- = 2$ (magenta) lines. Dotted lines: numerical results obtained with the Hill–Saville–Russel program.[24] Remaining system parameters are given in Table 1.

frequency mobility modulus spectra do not coincide because the former also depend on the concentration coefficient and the latter on the electroosmotic and capillary osmotic velocities that are certainly different in these two cases.

dx.doi.org/10.1021/jp3075404 | J. Phys. Chem. B 2012, 116, 13538–13553

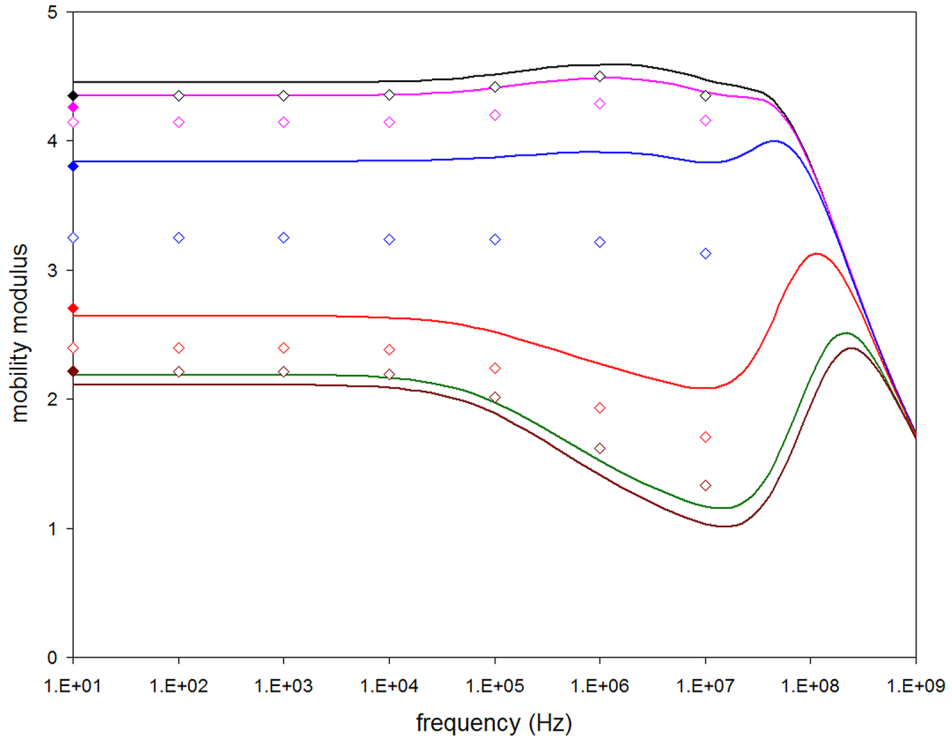

Figure 13. Electrophoretic mobility modulus spectra, eq 47, and their dependence on the stagnant layer parameters, considering that $z^+ = z^- = 1$. No stagnant layer (black), stagnant layer with $pK^+ = 1$ and $pK^- = -2$ (magenta), $= -1$ (blue), $= 0$ (red), $= 1$ (green), and $= 2$ (brown) lines. Empty diamonds: numerical results copied from the upper part of Figure 9 in ref 10; see text. Solid diamonds on vertical axis: numerical results obtained with the Mangelsdorf–White DC program.[8] Remaining system parameters are given in Table 1.

CONCLUSION

The original formulation of the Shilov–Dukhin theory presented in refs 1–3 provides analytical expressions suitable for the interpretation of DC and AC dielectric and electrokinetic data. However, besides the basic requirement for its validity that the radius of the particles must be much greater than the Debye screening length, the original results present a series of additional limitations:

(a) The valences of counterions and co-ions must have the same value.
(b) The frequency of the applied AC electric field must be relatively low (usually less than 1 MHz).
(c) The surface conductivity must only be due to the diffuse double layer so that the possibility of a stagnant layer conductivity is excluded.

These limitations made this theory unsuitable for the interpretation of a wide range of experimental data that therefore required the use of numerical calculations.

In a series of previous works, we individually addressed most of these limitations,[16−19] widening substantially the range of data that could be analytically interpreted. However, the stagnant layer conductivity was only included in DC fields and for equal counterion and co-ion valences. In this work, we extend this treatment to low and high frequency AC as well as for different counterion and co-ion valences. The end result is a unified and self-contained analytical theory of the dielectric and electrokinetic properties of colloidal suspensions that could be used over a broad frequency range, with particles allowed to have a stagnant layer conductivity, and suspended in electrolyte solutions with counterion and co-ion valences that can differ from one another.

The obtained expressions obviously reduce for the appropriate limits to the original formulation of the theory[1−3] and to the existing extensions.[16−19] They are also in good agreement with numerical data obtained by means of the Mangelsdorf–White program [8] (DC, different valences, stagnant layer) and the Hill–Saville–Russel program [24] (AC, different valences, no stagnant layer). A comparison with published Mangelsdorf–White numerical data [10] (AC, equal valences, stagnant layer) is inconclusive because of what appears to be a mistake in the captions of Figures 9 and 10 in that reference.

We hope that the presented analytical results might be useful for the interpretation of a broad range of experimental data, without having to rely on numerical calculations, and also as a starting point for further extensions of the theory.

AUTHOR INFORMATION

Corresponding Author

*E-mail: cgrosse@herrera.unt.edu.ar. Phone: +54-381-4251481.

Notes

The authors declare no competing financial interest.

ACKNOWLEDGMENTS

We are grateful to Prof. Lee White for the DC program,[8] to Dr. Christine Mangelsdorf for the AC program,[10] which unfortunately could not be used since it does not execute on current hardware, and to Prof. Reghan Hill for the AC program.[24] Financial support for this work by CIUNT (project 26/E419) is gratefully acknowledged.

REFERENCES

(1) Dukhin, S. S.; Shilov, V. N. Theory of the Static Polarization of the Diffuse Part of the Thin Double Layer of Spherical Particles. *Kolloidn. Zh.* **1969**, *31*, 706–713.

(2) Shilov, V. N.; Dukhin, S. S. Theory of Low-Frequency Dispersion of Dielectric Permittivity in Suspensions of Spherical Colloidal Particles due to Double-Layer Polarization. *Kolloidn. Zh.* **1970**, *32*, 293−300.
(3) Dukhin S. S.; Shilov V. N. *Dielectric Phenomena and the Double Layer in Disperse Systems and Polyelectrolytes*; Wiley: New York, 1974.
(4) Overbeek, J. Th. G. Theorie der Elektrophorese. Der Relaxationseffekt. *Kolloid-Beih.* **1942**, *54*, 287−364.
(5) O'Brien, R. W.; White, L. R. Electrophoretic Mobility of a Spherical Colloidal Particle. *J. Chem. Soc., Faraday Trans. 2* **1978**, *74*, 1607−1626.
(6) DeLacey, E. H. B.; White, L. R. Dielectric Response and Conductivity of Dilute Suspensions of Colloidal Particles. *J. Chem. Soc., Faraday Trans. 2* **1981**, *77*, 2007−2039.
(7) Mangelsdorf, C. S.; White, L. R. Dielectric Response of a Dilute Suspension of Spherical Colloidal Particles in an Oscillating Electric Field. *J. Chem. Soc., Faraday Trans. 2* **1997**, *93*, 3145−3154.
(8) Mangelsdorf, C. S.; White, L. R. Effects of Stern-Layer Conductance on Electrokinetic Transport Properties of Colloidal Particles. *J. Chem. Soc., Faraday Trans.* **1990**, *86*, 2859−2870.
(9) Mangelsdorf, C. S.; White, L. R. The Dynamic Double Layer. Part 1. Theory of the Mobile Stern Layer. *J. Chem. Soc., Faraday Trans.* **1998**, *94*, 2441−2452.
(10) Mangelsdorf, C. S.; White, L. R. The Dynamic Double Layer. Part 2. Effects of Stern-Layer Conduction on the High-Frequency Electrokinetic Transport Properties. *J. Chem. Soc., Faraday Trans.* **1998**, *94*, 2583−2593.
(11) Hinch, J. E.; Sherwood, J. D.; Chew, W. C.; Sen, P. N. Dielectric Response of a Dilute Suspension of Spheres with Thin Double Layers in an Asymmetric Electrolyte. *J. Chem. Soc., Faraday Trans. 2* **1984**, *80*, 535−551.
(12) O'Brien, R. W. The High-Frequency Dielectric Dispersion of a Colloid. *J. Colloid Interface Sci.* **1986**, *113*, 81−93.
(13) Shilov, V. N.; Delgado, A. V.; Gonzalez-Caballero, F.; Grosse, C. Thin Double Layer Theory of the Wide-Frequency Range Dielectric Dispersion of Suspensions of Non-Conducting Spherical Particles Including Surface Conductivity of the Stagnant Layer. *Colloids Surf. A* **2001**, *192*, 253−265.
(14) Simonova, T. S.; Shilov, V. N. Influence of the Mobility of Ions of the Dense Portion of an Electric Double Layer of Spherical Particles on Electrophoresis and Electrical Conductivity of Disperse Systems. *Kolloidn. Zh.* **1986**, *48*, 370−373.
(15) Lyklema, J.; Minor, M. On the Surface Conduction and its Role in Electrokinetics. *Colloids Surf. A* **1998**, *140*, 33−41.
(16) Grosse, C. Generalization of a Classic Thin Double Layer Polarization Theory of Colloidal Suspensions to Electrolyte Solutions with Different Ion Valences. *J. Phys. Chem. B* **2009**, *113*, 8911−8924.
(17) Grosse, C. Generalization of a Classic Theory of the Low Frequency Dielectric Dispersion of Colloidal Suspensions to Electrolyte Solutions with Different Ion Valences. *J. Phys. Chem. B* **2009**, *113*, 11201−11215.
(18) Grosse, C. Extension of a Classic Theory of the Low Frequency Dielectric Dispersion of Colloidal Suspensions to the High Frequency Domain. *J. Phys. Chem. B* **2010**, *114*, 12520−12527.
(19) Grosse, C. Extension of a Classic Thin Double Layer Polarization Theory of Colloidal Suspensions to Include the Stagnant Layer Conductivity. *J. Phys. Chem. B* **2010**, *115*, 8996−9004.
(20) Bikerman, J. J. Electrokinetic Equations and Surface Conductance. A Survey of the Diffuse Double Layer Theory of Colloidal Solutions. *Trans. Faraday Soc.* **1940**, *35*, 154−160.
(21) Maxwell, J. C. A *Treatise on Electricity and Magnetism*; Clarendon Press: Oxford, U.K., 1892; Vol. *1*.
(22) Wagner, K. W. Erklärung der Dielektrischen Nachwirkungsvorgänge auf Grund Maxwellscher Vorstellungen. *Arch. Elektrotech.* **1914**, *2*, 371−387.
(23) O'Konski, C. T. Electric Properties of Macromolecules. V. Theory of Ionic Polarization in Polyelectrolytes. *J. Phys. Chem.* **1960**, *64*, 605−619.
(24) Hill, R. J.; Saville, D. A.; Russel, W. B. Polarizability and Complex Conductivity of Dilute Suspensions of Spherical Colloidal Particles with Uncharged (Neutral) Polymer Coatings. *J. Colloid Interface Sci.* **2003**, *268*, 230−245.
(25) Pedrosa, S. E.; Grosse, C. Numerical Analysis of the Concentration Polarization in Colloidal Suspensions: Comparison with Theoretical Predictions. *J. Colloid Interface Sci.* **1999**, *219*, 37−47.
(26) Lopez-Garcia, J. J.; Grosse, C.; Horno, J. Influence of the Counterion and Co-Ion Diffusion Coefficient Values on some Dielectric and Electrokinetic Properties of Colloidal Suspensions. *J. Phys. Chem. B* **2005**, *109*, 11907−11912.
(27) O'Brien, R. W. Electro-Acoustic Effects in a Dilute Suspension of Spherical Particles. *J. Fluid Mech.* **1988**, *190*, 71−86.
(28) Ahualli, S.; Delgado, A. V.; Grosse, C. A Simple Model of the High-Frequency Dynamic Mobility in Concentrated Suspensions. *J. Colloid Interface Sci.* **2006**, *301*, 660−667.